Computers and Geotechnics 168 (2024) 106188

Contents lists available at ScienceDirect

Computers and Geotechnics

journal homepage: www.elsevier.com/locate/compgeo

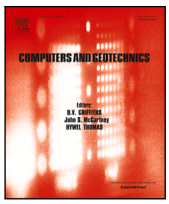

Research paper

Non-linear behaviour of soil–pile interaction phenomena and its effect on the seismic response of OWT pile foundations. Validity range of a linear approach through non-degraded soil properties

Eduardo Rodríguez-Galván, Guillermo M. Álamo *, Juan J. Aznárez, Orlando Maeso

Instituto Universitario de Sistemas Inteligentes y Aplicaciones Numéricas en Ingeniería, Universidad de Las Palmas de Gran Canaria, 35017 Las Palmas de Gran Canaria, Spain

ARTICLE INFO

Keywords:
Soil–pile interaction
Non-linear analysis
Inelastic behaviour
Offshore wind turbines
Beam on dynamic Winkler foundation
Seismic response

ABSTRACT

The effect of non-linear and inelastic behaviour of the soil–pile interaction on the seismic response of offshore wind turbine pile foundations embedded in sandy soils is analysed. For this purpose, the responses obtained assuming three different Beam on Dynamic Winkler Foundation (BDWF) models are compared: a Plastic Non-Linear Model (PNLM), an Elastic Non-Linear Model (ENLM) and a simple elastic linear model with non-degraded properties of soil (NDLM). The influence of non-linearity and plasticity assumption is studied by evaluating the effects of the kinematic and inertial interaction within soil–pile interaction. Two soil stiffness levels are analysed: very loose and medium dense sand. The seismic response under ten earthquakes is computed in terms of mean envelopes of internal forces along the pile length. The non-linearity and inelastic influence of soil–pile interaction is quantified by means of relative differences with respect to the linear elastic model. Results show that the non-linear and inelastic models acquire relevance when the contribution of the inertial interaction dominates, leading to lower maximum responses than the linear elastic model. If the inertial interaction is not significantly activated, similar results between the three models are obtained, being the linear elastic model enough to reproduce the soil–pile dynamic interaction.

1. Introduction

One of the most relevant applications of piled foundations is its use in offshore wind turbine (OWT) structures. Monopiles are the dominant OWT foundation, representing 64.4% of the total OWTs foundation market for installed projects in 2021 (Musial et al., 2022). This type of foundation predominates due to its ease of installation and manufacturing, which make it a very economically competitive solution. Monopiles with larger dimensions are evolving to increase its range of application, both in seabed depths and in supporting high-powered wind turbines. The new generation of OWTs ($\geq$ 15 MW) requires monopiles with more than 10 meters in diameter and 100 meters in length. For smaller OWTs, monopiles acquire diameters of up to 8 m and lengths of up to 90 m (BOSLAN Engineering and Consulting, 2022). In addition, piles are also very present in the rest of the OWT bottom-fixed foundations. Jackets, tripods and tripiles substructures are founded on suction caissons or on smaller sized piles, which generally have diameters between 1 and 4 m and lengths from 25 to 80 m. In this way, piles can acquire a great variety of sizes depending on the type of OWT foundation.

The wide expansion of the offshore wind technology has led to considering its installation in seismically active regions with more aggressive environmental conditions. For this reason, with the aim of analysing the dynamic-structural response of bottom-fixed OWTs, numerous dynamic studies have been carried out in recent years (Shi et al., 2022; Liang et al., 2022; Wang et al., 2018; Yang et al., 2019; Xi et al., 2022; Mo et al., 2021; Patra and Haldar, 2021; Padrón et al., 2022; Medina et al., 2021; Kaynia, 2021; Álamo et al., 2018; Jiang and Lin, 2022; Jiang et al., 2021; Bisoi and Haldar, 2014; Ju and Huang, 2019; Yan et al., 2022; Alati et al., 2015; Hassan, 2018; Carswell et al., 2016; Bisoi and Haldar, 2015; Wang et al., 2023). In many of these studies (Shi et al., 2022; Yang et al., 2019; Padrón et al., 2022; Medina et al., 2021; Kaynia, 2021; Álamo et al., 2018), especially those that focus on monopiles, the relevance of soil–structure interaction in the structural behaviour is demonstrated, both in the dynamic properties of the systems (natural frequencies, damping, etc.) and its responses. The dynamic soil–structure interaction essentially includes kinematic and inertial interaction. Kinematic interaction is mainly affected by

* Corresponding author.
E-mail addresses: eduardo.rodriguezgalvan@ulpgc.es (E. Rodríguez-Galván), guillermo.alamo@ulpgc.es (G.M. Álamo), juanjose.aznarez@ulpgc.es (J.J. Aznárez), orlando.maeso@ulpgc.es (O. Maeso).

https://doi.org/10.1016/j.compgeo.2024.106188
Received 17 November 2023; Received in revised form 2 February 2024; Accepted 22 February 2024
Available online 24 February 2024

soil motion and soil–pile interface, while inertial interaction is mainly associated to the mass of the superstructure.

The seismic and dynamic analysis of OWTs can be carried out assuming a linear or non-linear soil–structure interaction. Although it is more complex, the non-linear behaviour is commonly used (Shi et al., 2022; Liang et al., 2022; Wang et al., 2018; Yang et al., 2019; Xi et al., 2022; Mo et al., 2021; Jiang and Lin, 2022; Jiang et al., 2021; Bisoi and Haldar, 2014; Hassan, 2018; Patra and Haldar, 2021; Carswell et al., 2016; Bisoi and Haldar, 2015; Wang et al., 2023), because it is considered a more realistic approach than the linear one. In these type of numerical simulations, the soil–pile dynamic interaction is usually represented by a non-linear Beam on Dynamic Winkler Foundation (BDWF) model with springs in parallel with dashpots, that can be considered elastic or plastic. In these BDWF models the soil resistance - deflection (p-y) relationship is usually modelled by using the API (Designing API RP 2A-WSD, 2002) expressions (Hassan, 2018; Carswell et al., 2016; Bisoi and Haldar, 2015; Wang et al., 2023; Bisoi and Haldar, 2014; Wang et al., 2018; Mo et al., 2021; Shi et al., 2022). Although this API method has not been designed to simulate the p-y curves for large diameter piles, its application has been recommended by several design guidelines, as the DNV-OS-J101 (DNV, 2014a), and it has been widely employed in the dynamic study of monopile-supported OWTs, as well as in prominent works such as the OC3 project (Jonkman and Musial, 2010), where the soil–pile dynamic interaction of the NREL 5MW OWT (6 m diameter pile) is reproduced by employing the API method.

On the other hand, linear models have also been used in numerous studies (Padrón et al., 2022; Medina et al., 2021; Kaynia, 2021; Álamo et al., 2018; Arany et al., 2016), and they may be a necessary and sufficient approximation depending on the case and phenomenon to be addressed. In these linear approaches, the soil–pile dynamic interaction is usually modelled by a set of impedance functions and kinematic interaction factors. Despite being simplified models, they are useful when a large number of simulations have to be addressed, and they are generally accepted as a initial approach. Regardless of the fact that both approaches have been studied in detail, many few works have focused on comparing them: Firoj and Maheshwari (2022) compares two linear soil behaviours with two non-linear ones, for combined piled raft foundation of a Nuclear Power Plant structure; Cheng et al. (2023) employs an elastoplastic and a elastic soil to analyse the dynamic response of a monopile-supported OWT in clay; and Tabesh and Poulos (2001) analyses the effects of soil yielding on the seismic response of small piles (up to 1.5 m diameter) embedded in clay and sandy soils, comparing an elastic and an elastoplastic soil–pile interaction.

For this reason, in the absence of an exhaustive comparison between these considerations, this paper aims to compare the structural-seismic response of OWT pile foundations embedded in sandy soils considering three different soil–pile interaction models: a Plastic Non-Linear Model (PNLM), an Elastic Non-Linear Model (ENLM) and a simple elastic linear model with non-degraded properties of soil (Non-Degraded Linear Model, NDLM). These three models have been specifically designed for isolating the influence of the soil–pile interaction. Thus, all the differences obtained in the results can be directly explained by the assumptions made for the soil–pile interaction phenomena. This fact allows to focus on the main scope of this work: the analysis of the effects of assuming a linear or non-linear (either inelastic or elastic) behaviour in the soil–pile interaction for evaluating seismic loads, and how this influence depends on the contribution of the inertial properties of the structure. In order to obtain general trends and useful conclusions that can help to choose the appropriate model depending on the interest problem, an exhaustive parametric study for a wide range of excitations and OWT pile foundations is carried out.

In the three models under analysis, the soil–pile interaction is represented by a BDWF approach based on the p-y curves recommended by the API RP 2A-WSD (Designing API RP 2A-WSD, 2002). Vertically incident S waves that propagates through an elastic medium with linear variation of soil properties with depth is considered in each model. In this way, the effect of non-linear and inelastic behaviour of soil–pile interaction is isolated and analysed. Besides, the relevance of the soil properties is also studied by considering two stiffness levels: a very loose and a medium dense sandy soil (following the API sandy soil classification (Designing API RP 2A-WSD, 2002)). In order to examine the role of the kinematic and inertial effects on the non-linear and inelastic soil–pile behaviour, different single piles with several cap masses values from 0 to the mass equivalent to its ultimate axial bearing capacity are studied. Results are presented in terms of envelopes of maximum internal forces, accelerations and soil resistances. To better quantify the relevance of the non-linear and plastic behaviour of soil–pile interaction, the relative differences of the maximum seismic responses with respect to those corresponding to the linear elastic model are computed. Finally, the conclusions drawn of this analysis are tested with three reference monopiled OWTs of different rated powers (5, 10 and 15 MW), comparing the envelopes of the three OWTs with those of its corresponding monopiles with a pile cap mass equivalent to its supported superstructure weight.

2. Methodology

The seismic response of the soil-monopile system is obtained through a BDWF model, the pile is discretized by beam finite elements, and the soil–pile interaction is reproduced through independent springs attached to each node of pile elements (Fig. 1). To study the effects of non-linearity and the consideration of the plastic-cyclic behaviour of soil–pile interaction, the three different models studied are (Fig. 1(a)): a Plastic Non-Linear Model (PNLM), an Elastic Non-Linear Model (ENLM) and a Non-Degraded Linear Model (NDLM). In order to limit the study to the relevance of the plastic and non-linear behaviour of soil–pile interaction, the gap formation between the soil–pile is not considered. In these three models, the seismic excitation is assumed to be a planar and harmonic S-wave vertically propagating through an elastic non-homogeneous halfspace with linear variation of soil properties with depth. Only the system seismic response is analysed (no environmental loads due to wind or waves are considered).

First, in order to study the kinematic and inertial effects in soil–pile interaction, several values of translational cap masses (m) are studied in a soil–pile subsystem (see Fig. 1(b)) by considering the three soil–pile models previously introduced. On this manner, the influence of the non-linear and inelastic behaviour of soil–pile interaction is analysed. These translational masses (m) are defined as a fraction (δ) of the ultimate axial bearing capacity of piles (Q_u). Finally, the application of the main conclusions drawn of this study are verified by using an integrated system that includes different reference monopiled OWTs (see Fig. 1(c)). In this section, the methodology followed to define the different systems and models is explained.

2.1. System modelling

The pile and wind turbine are discretized into finite elements of two nodes (Bernoulli's beams). Therefore, the soil–pile interface is concentrated into the beam axis, and consequently the local effects produced at the soil-shell interface are not captured. This simplification has been verified in previous works, such as in Álamo et al. (2021), which concludes that a soil-beam model accurately reproduces the global foundation response for not excessively high frequencies, even for foundations with small aspect ratios (L/D). Given the particularities of the problem, only the lateral behaviour of the system is considered. Thus, each node n has two degrees of freedom: a lateral displacement (u_n) and a rotation (θ_n). Distributed inertial properties are assumed for each element. Based on a convergence study, an element length (L_e) of 0.5 m and 1 m have been chosen to discretize the foundation (embedded pile) and the supestructure respectively, so that the soil–pile interaction and the conical shape of the tower are reproduced

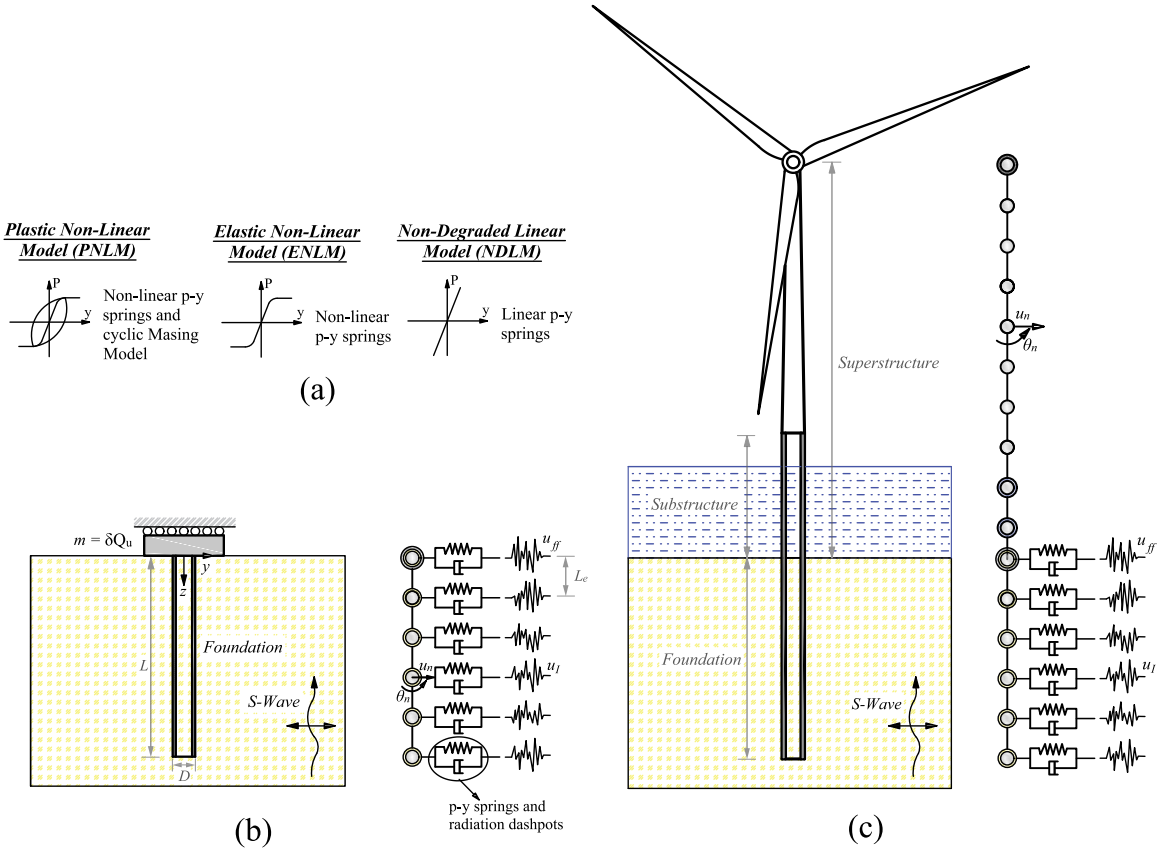

Fig. 1. (a) Soil–pile interaction models studied in this work. (b) Soil–pile subsystem for kinematic and inertial effects parametric analysis. (c) Integrated model including OWT superstructure.

accurately enough. For the soil–pile subsystem the pile cap mass (m) is modelled as a punctual and translational mass at the top node (pile head rotation is assumed to be restricted, as depicted in Fig. 1(b)). In the integrated system with the OWT superstructure the mass of the rotor-nacelle assembly is also considered as a punctual mass at the highest node. In this last model, the transition piece between the monopile and the tower is not taken into account for simplification reasons (see Fig. 1(c)).

The classic Bernoulli's stiffness and elementary mass matrices ($\mathbf{K_e}$ and $\mathbf{M_e}$) used for each element are shown in (1) and (2), being L_e the element length, A_e the cross-sectional area of the element, I_e the moment of inertia of the cross-section, ρ the material density and E the Young's Modulus of the material. For the soil–pile subsystem and for the integrated system including OWT superstructure, the equivalent soil mass inside the foundation is considered as an added distributed elementary mass. For the integrated model with OWT superstructure the interaction between the monopile and the water is modelled as two added distributed elementary masses: one for the water inside the pile and another for the mobilized water outside the substructure, as it is described in (3), being ρ_w the water density, A_{in} and A_{out} the circle areas corresponding to the inner and outside diameters of the pile section, and C_a an added mass coefficient that, for long cylinders in infinite fluid, takes a value of 1 following the DNV-RP-C205 (DNV, 2014b). It is important to consider these two water added masses, since they can significantly affect the first natural system frequency, as it is demonstrated in Chen et al. (2022). All these elemental matrices are assembled to obtain the global stiffness and mass matrices of the system.

$$\mathbf{K_e} = \frac{EI_e}{L_e^3}\begin{bmatrix} 12 & 6L_e & -12 & 6L_e \\ 6L_e & 4L_e^2 & -6L_e & 2L_e^2 \\ -12 & -6L_e & 12 & -6L_e \\ 6L_e & 2L_e^2 & -6L_e & 4{L_e}^2 \end{bmatrix} \tag{1}$$

$$\mathbf{M_e} = \frac{\rho A_e L_e}{420}\begin{bmatrix} 156 & 22L_e & 54 & -13L_e \\ 22L_e & 4L_e^2 & 13L_e & -3L_e^2 \\ 54 & 13L_e & 156 & -22L_e \\ -13L_e & -3L_e^2 & -22L_e & 4{L_e}^2 \end{bmatrix} \tag{2}$$

$$\mathbf{M_{ew}} = \frac{\rho_w L_e (A_{in} + C_a A_{out})}{420}\begin{bmatrix} 156 & 22L_e & 54 & -13L_e \\ 22L_e & 4L_e^2 & 13L_e & -3L_e^2 \\ 54 & 13L_e & 156 & -22L_e \\ -13L_e & -3L_e^2 & -22L_e & 4{L_e}^2 \end{bmatrix} \tag{3}$$

2.2. Dynamic soil–pile interaction models

In this work, in order to study the effects of non-linear and inelastic behaviour of soil–pile interaction, three different models are studied: a Plastic Non-Linear Model (PNLM), an Elastic Non-Linear Model (ENLM) and a Non-Degraded Linear Model (NDLM).

2.2.1. Plastic Non-Linear Model (PNLM)

In this model, the lateral soil resistance-deflection is modelled using the non-linear p-y relationship for sands, established and recommended by the API (Designing API RP 2A-WSD, 2002):

$$P = Ap_u \tanh\left[\frac{kz}{Ap_u}\tilde{y}\right] \tag{4}$$

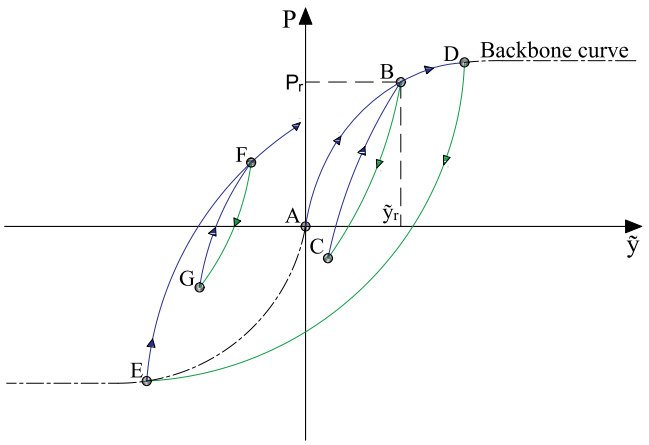

Fig. 2. Extended masing rules, example of the evolution of soil resistance (P) versus soil–pile relative displacement ($\tilde{y}$).

where P is the reaction force of soil per unit length; $\tilde{y}$ is the soil–pile relative displacement ($\tilde{y} = u - u_I$), defined as the difference between the lateral displacement of the pile (u) and that of the soil due to the incident field (u_I); A is a dimensionless coefficient which depends on the type of loading, in this case, A is taken as 0.9 (cyclic loading); k is the initial modulus of subgrade reaction, that can be graphically calculated as function of angle of internal friction (Φ_s) with Figure 6.8.7-1 of API RP 2A-WSD (Designing API RP 2A-WSD, 2002); and p_u is the ultimate bearing capacity at depth z, which is computed according to:

$$p_u = \min(p_{us}, p_{ud}) \tag{5}$$

where:

$$p_{us} = (C_1 z + C_2 D)\gamma_s z \tag{6}$$

and

$$p_{ud} = C_3 D \gamma_s z \tag{7}$$

being γ_s the effective soil weight; D the pile diameter; and C_1, C_2, C_3 dimensionless coefficients which are functions of Φ_s and can be determined with Figure 6.8.6-1 of API RP 2A-WSD (Designing API RP 2A-WSD, 2002).

To model the plastic-cyclic behaviour of soil–pile interaction, the non-linear p-y relationship of soil is modelled by using a cyclic extended Masing model, in which the backbone curve is described by (4). These types of cyclic non-linear models are very common to simulate the stress–strain hysteretic behaviour of soil, since they can reproduce the unloading-reloading behaviour, stiffness degradation and other effects (Gerolymos and Gazetas, 2005b,a). The four Masing rules that define the cyclic model are (see e.g. Kramer (1996)):

1. For initial loading, the p-y curve follows the backbone curve (from A to B in Fig. 2).
2. If a deflection reversal occurs at a point defined by (P_r, $\tilde{y}_r$) (point B in Fig. 2), the p-y curve follows a path given by:

$$P = P_r + 2Ap_u \tanh\left[\frac{kz}{Ap_u}\frac{\tilde{y} - \tilde{y}_r}{2}\right] \tag{8}$$

3. If the unloading or reloading curve exceeds the maximum past deflection and intersects the backbone curve, it follows the backbone curve until the next deflection reversal (from C to D in Fig. 2).
4. If an unloading or reloading curve crosses an unloading or reloading curve from the previous cycle, the p-y curve follows that of the previous cycle (from G to F in Fig. 2).

In this way, in each time step, using the Newmark non-linear method (Section 2.6.2) with the correct p-y curve ((4) or (8) depending on the path given by the Masing Rules), displacements, velocities and accelerations of the system are computed.

2.2.2. Elastic Non-Linear Model (ENLM)

In this model, as in the previous one, the non-linear relationship between the lateral soil resistance-deflection is computed by means of the API p-y curve for sands. However, an elastic soil behaviour is considered. Thus, Masing rules are not applied and the p-y relationship is limited to the original backbone curve (dashed line in Fig. 2). Therefore, in each time step, applying Newmark non-linear method (Section 2.6.2) with the p-y curve (4), displacements, velocities and accelerations of the system are calculated.

2.2.3. Non-Degraded Linear Model (NDLM)

A linear relationship between the lateral soil resistance-deflection is considered in this model. This linear relationship is defined as the initial slope of the p-y curve (4) at $\tilde{y} = 0$ m. Thus, the linear relation between the soil reaction per unit length (P) and lateral soil–pile relative displacement ($\tilde{y}$) is:

$$P = kz\tilde{y} \tag{9}$$

2.3. System damping

System material damping is considered following the Rayleigh approach, so the damping matrix $\mathbf{C_M}$ can be computed by (see e.g. Chopra (2011)):

$$\mathbf{C_M} = A\mathbf{M_m} + B\mathbf{K_m} \tag{10}$$

where $\mathbf{M_m}$ and $\mathbf{K_m}$ are the global stiffness and mass matrices of the system (without considering the interaction with the soil and the water). Parameters A and B are calculated as:

$$A = \zeta \frac{2\omega_i \omega_j}{\omega_i + \omega_j} \tag{11}$$

$$B = \zeta \frac{2}{\omega_i + \omega_j} \tag{12}$$

being ω_i and ω_j the natural frequencies, and ζ the damping fraction for the i^{th} and j^{th} modes. In this work, the first and last modes are chosen and a damping value of 2% is considered.

In order to model the loss of the energy transmitted from the foundation to the soil, a radiation damping in parallel with lateral soil–pile spring is contemplated. Considering that the soil is nearly incompressible, this radiation damping per unit length can be calculated following (Gazetas and Dobry, 1984):

$$c_r = 4D\rho_s V_s \tag{13}$$

being D the pile diameter; ρ_s and V_s the density and shear wave velocity of soil respectively. With these radiation and material dampings, the global damping matrix of the system is determined.

2.4. Seismic input incident field

The system is excited by planar shear waves that propagate vertically through the soil acting in the y direction, producing a free-field (without foundation) lateral displacement at ground level that is denoted as u_{ff}. The harmonic incident field is assumed to propagate through a non-homogeneous medium with continuous variation of soil properties with depth and linear behaviour.

For a continuously non-homogeneous soil with a single layer, the horizontal displacements (u_I) in frequency domain due to the incident field can be computed following the expressions proposed by

Rovithis et al. (2011), where the shear wave propagation velocity (V_s) is determined according to the generalized power-law function:

$$V_s(z) = V_r \left(b + q \frac{z}{z_r} \right)^n \tag{14}$$

being z the depth from ground surface; V_r and z_r the reference shear wave velocity and depth respectively (established at 15 m); $b = (V_0/V_s)^{1/n}$ and $q = 1 - b$ the parameters that determine the shear wave velocity at surface level (V_0); and n the parameter that determines the evolution of the shear wave with depth. In this work, in order to follow the same profile represented by the API curves (linear variation with depth of the soil shear modulus), the values $V_0 = 0$ m/s and $n = 0.5$ are considered.

The lateral displacements at a certain level and frequency ($u_I(z,\omega)$) due to an incident field propagating in a non-homogeneous medium with these characteristics is determined by the following equation established in Rovithis et al. (2011):

$$u_I(z,\omega) = \frac{C_1 (b + qz/z_r)^\mu}{N_{\nu+1}(\lambda b^{\ell/2})} \left\{ J_\nu \left[\lambda \left(b + q \frac{z}{z_r} \right)^{\ell/2} \right] N_{\nu+1} \left(\lambda b^{\ell/2} \right) - J_{\nu+1} \left(\lambda b^{\ell/2} \right) N_\nu \left[\lambda \left(b + q \frac{z}{z_r} \right)^{\ell/2} \right] \right\} \tag{15}$$

where C_1 is a boundary constant; J_ν and N_ν are the Bessel functions of the first and second kind and order ν respectively; ℓ, μ and ν are dimensionless parameters defined as $\ell = 2(1-n)$, $\mu = (1-2n)/2$ and $\nu = (2n-1)/(2(1-n))$; and $\lambda = 2k_I z_r/(\ell q)$ is the wave length corresponding to the wave number $k_I = \omega/V_r$.

With the displacements $u_I(z,\omega)$ calculated, the velocities $v_I(z,\omega)$ due to the seismic excitation in the frequency domain are determined:

$$v_I(z,\omega) = \mathrm{i}\omega u_I(z,\omega) \tag{16}$$

once the horizontal displacements and velocities are computed in frequency domain, they are obtained in time domain employing the frequency domain method. For this purpose, the frequency response functions of displacements and velocities at the desired depths with respect to the free field displacement are computed by using (15).

2.5. Ultimate axial bearing capacity

In this section, the methodology followed to compute the different cap translational masses (m) studied for the soil–pile subsystem (Fig. 1(b)) is explained. As it has been mentioned, the values adopted for these cap masses are a fraction (δ) of the ultimate axial bearing capacity (Q_u) of the piles, that is computed following the API (Designing API RP 2A-WSD, 2002):

$$Q_u = Q_f + Q_p = f A_s + q A_p \tag{17}$$

being Q_f the skin friction resistance, Q_p the total end bearing, f the unit skin friction capacity, A_s the side surface area of pile, q the unit end bearing capacity and A_p the gross end area of pile.

If the pile is unplugged, the shaft friction f acts on both inside and outside the pile, for plugged piles this shaft friction only acts on outside the pile. On this manner, the ultimate axial bearing capacity for unplugged piles is computed as the sum of the outside and inside skin friction resistance and the total end bearing corresponding to the annular section of the pile; while for plugged piles this ultimate bearing capacity is calculated as the sum of the external skin friction resistance and the total end bearing of the entire cross section of the pile. To determine if the pile is plugged or unplugged, the minimal value of the Q_u for unplugged and plugged pile is selected, as it is established in the API.

The shaft friction f, for piles in cohesionless soils, can be computed as:

$$f = K p_o \tan \delta_s \tag{18}$$

where K is the coefficient of lateral earth pressure, that takes a value of 0.8 and 1 for unplugged and plugged piles, respectively; p_o is the effective overburden pressure at the point in question, that is the product of the soil density and depth; and δ_s the friction angle between the soil and pile wall (whose values are described in the Table 6.4.3-1 of the API (Designing API RP 2A-WSD, 2002)). This shaft friction f is assumed to linearly increase with the overburden pressure until a limiting skin friction value is reached (f_{lim}, whose value is also established in Table 6.4.3-1 of API).

The unit end bearing q for cohesionless soils can be computed as:

$$q = p_o N_q \tag{19}$$

being N_q a dimensionless bearing capacity factor. The value of q is also limited by a unit end bearing value (q_{lim}, Table 6.4.3-1 of API).

2.6. Dynamic analysis

The time response of the system under variable loads can be computed by using the dynamic equation of motion in finite elements:

$$\mathbf{M}\ddot{\vec{u}}(t) + \mathbf{C}\dot{\vec{u}}(t) + \mathbf{K}\vec{u}(t) = \vec{F}(t) \tag{20}$$

where $\vec{u}$, $\dot{\vec{u}}$, $\ddot{\vec{u}}$ are the nodal displacements, velocities and accelerations, respectively; $\mathbf{M}$, $\mathbf{C}$, $\mathbf{K}$ are the mass, damping and stiffness matrices of the system; $\vec{F}$ is the nodal force vector; and t is the time. To solve (20) the Newmark Method is employed (see e.g. Chopra (2011)). In this study, the average acceleration method is considered. The nodal force vector ($\vec{F}$) is composed of the elastic and damping linear forces that the soil–pile interaction exerts on the pile due to the incident field.

Once displacements, velocities and accelerations of the system have been computed, with the stiffness, mass, damping matrices of each element, and by using (20), internal forces of each element are determined (shear forces $\vec{V}$ and bending moments $\vec{M}$).

2.6.1. Linear system resolution

Newmark Method for linear systems is used to compute displacements, velocities and accelerations for the NDLM. According to this method, the displacement in the time step ($\vec{u}_{t+1}$) can be calculated by:

$$\left(\mathbf{K} + \frac{\gamma}{\beta \Delta t}\mathbf{C} + \frac{1}{\beta(\Delta t)^2}\mathbf{M} \right) \vec{u}_{t+1} = \hat{\vec{F}}_{t+1} \tag{21}$$

where Δt is the time step and $\hat{\vec{F}}_{t+1}$ is the equivalent force vector at time $t+1$, which can be computed from the response of the previous time instant as:

$$\hat{\vec{F}}_{t+1} = \vec{F}_{t+1} + \left[\frac{1}{\beta(\Delta t)^2}\mathbf{M} + \frac{\gamma}{\beta \Delta t}\mathbf{C} \right] \vec{u}_t + \left[\frac{1}{\beta(\Delta t)}\mathbf{M} + \left(\frac{\gamma}{\beta} - 1 \right)\mathbf{C} \right] \dot{\vec{u}}_t + \left[\left(\frac{1}{2\beta} - 1 \right)\mathbf{M} + \Delta t \left(\frac{\gamma}{2\beta} - 1 \right)\mathbf{C} \right] \ddot{\vec{u}}_t \tag{22}$$

once $\vec{u}_{t+1}$ is computed, the velocities and accelerations in the next time step ($\dot{\vec{u}}_{t+1}$ and $\ddot{\vec{u}}_{t+1}$ respectively) are determined using:

$$\dot{\vec{u}}_{t+1} = \frac{\gamma}{\beta \Delta t}(\vec{u}_{t+1} - \vec{u}_t) + \left(1 - \frac{\gamma}{\beta} \right)\dot{\vec{u}}_t + \Delta t \left(1 - \frac{\gamma}{2\beta} \right)\ddot{\vec{u}}_t \tag{23}$$

$$\ddot{\vec{u}}_{t+1} = \frac{1}{\beta(\Delta t)^2}(\vec{u}_{t+1} - \vec{u}_t) - \frac{1}{\beta \Delta t}\dot{\vec{u}}_t - \left(\frac{1}{2\beta} - 1 \right)\ddot{\vec{u}}_t \tag{24}$$

2.6.2. Non-linear system resolution

Newmark Method for non-linear system is used to solve (20) in non-linear models (PNLM and ENLM). This method is based on iterating the value of the displacement until a solution of the non-linear equilibrium equation is achieved. The main equation governing this method is (see e.g. Chopra (2011)):

$$(\hat{\mathbf{K}}_T)^{(j)}_{t+1} \vec{\Delta u}^{(j)} \equiv \hat{\vec{R}}^{(j)}_{t+1} \tag{25}$$

Table 1
Main characteristics of soils considered in this work.

	Very loose sand (Loose)	Medium dense sand (Dense)
Poisson's ratio [ν_s]	0.49	0.49
Density [ρ_s] (kg/m^3)	2000	2000
Shear wave velocity [V_s] (m/s)	92.41	232.56
Angle of internal friction [Φ] (°)	28	36
Initial modulus of subgrade reaction [k] (MN/m^3)	4.07	25.79
C_1	1.60	3.30
C_2	2.40	3.60
C_3	22	60
Soil-pile friction angle [δ_s] (°)	15	25
Limiting skin friction value [f_{lim}] (kN/m^2)	47.8	81.3
N_q	8	20
Limiting unit end bearing value [q_{lim}] (MN/m^2)	1.9	4.8

being $(\hat{\mathbf{K}}_T)^{(j)}_{t+1}$ the tangent stiffness for the j^{th} iteration in the next time step $t+1$; $\vec{\Delta u}^{(j)}$ the variation of displacement; and $\hat{\vec{R}}^{(j)}_{t+1}$ the residual force. All these terms must be updated in each iteration and time step following:

$$(\hat{\mathbf{K}}_T)^{(j)}_{t+1} \equiv (\hat{\mathbf{K}}_T)^{(j)}_{t+1} + \frac{\gamma}{\beta \Delta t}\mathbf{C} + \frac{1}{\beta(\Delta t)^2}\mathbf{M} \tag{26}$$

$$\vec{\Delta u}^{(j)} = \vec{u}^{(j+1)}_{t+1} - \vec{u}^{(j)}_{t+1} \tag{27}$$

$$\hat{\vec{R}}^{(j)}_{t+1} = \vec{F}_{t+1} - (\vec{F}_S)^{(j)}_{t+1} - \left[\frac{1}{\beta(\Delta t)^2}\mathbf{M} + \frac{\gamma}{\beta \Delta t}\mathbf{C}\right]\left(\vec{u}^{(j)}_{t+1} - \vec{u}_t\right) + \left[\frac{1}{\beta \Delta t}\mathbf{M} + \left(\frac{\gamma}{\beta} - 1\right)\mathbf{C}\right]\dot{\vec{u}}_t + \left[\left(\frac{1}{2\beta} - 1\right)\mathbf{M} + \Delta t\left(\frac{\gamma}{2\beta} - 1\right)\mathbf{C}\right]\ddot{\vec{u}}_t \tag{28}$$

where the term $(\vec{F}_S)^{(j)}_{t+1}$ is the restoration force, that is, the elastic force. The initialization of the iteration is carried out considering a displacement equal to that of the previous time instant.

After each iteration, the solution is verified and the iterative process ends when a measure of error is less than a specified tolerance. In this work, the convergence criterion is established in terms of the norm of the difference of the displacement vectors between iterations:

$$|\vec{\Delta u}^{(j)}| \leq \varepsilon_u \tag{29}$$

being ε_u the tolerance, fixed as 10^{-10} m. Once the tolerance criterion is fulfilled, the velocities and accelerations are computed following (23) and (24).

3. Problem definition

3.1. Soil properties

A very loose (Loose) and a medium dense (Dense) sandy soils are considered in this study. Each soil is assumed to be a halfspace, where the lateral bearing capacity and the soil resistance deflection relationship varies with depth following the API expressions. The main characteristics of each soil type are shown in Table 1, together with the values assumed for the definition of the API *p-y* curves and the Q_u calculation.

3.2. Pile properties

In order to analyse typical piles of OWT foundations, three different piles with diameters $D = 0.5, 1$ and 5 m are studied. For all piles, a length $L = 30$ m is considered. In this way, small piles (typical of jackets) and larger piles (typical of monopiles) are included. Two more lengths ($L = 15$ and 60 m) are considered for the pile with $D = 1$ m. The thickness of each pile (t_p) is determined by the expression proposed by the API RP 2A-WSD (Designing API RP 2A-WSD, 2002):

$$t_p \geq 6.35 + \frac{D}{100}\ [\text{mm}] \tag{30}$$

Table 2
Main characteristics of the piles studied in this work.

D (m)	L (m)	t_p (mm)	Q_u (t) - Loose	Q_u (t) - Dense	Plugged/Unplugged
0.5	30	11.35	232.8	428.8	Plugged
1	15	16.35	290.4	508.6	Unplugged
	30	16.35	541.8	1050	Plugged
	60	16.35	1001	1831	Plugged
5	30	56.35	3850	6721	Unplugged

The cap masses (m) analysed in the soil–pile subsystem (see Fig. 1(b)) are defined as a fraction (δ) of the ultimate bearing capacity (Q_u), ranging from $\delta = 0$ to 1, with steps of 0.125. The main information about the piles analysed in this work, along with the ultimate axial bearing capacity (Q_u) of each pile and soil is presented in Table 2.

3.3. OWT properties

Three reference OWTs with rated powers of 5, 10 and 15 MW and its corresponding monopiles are analysed in this study. The main characteristics of these OWTs and monopiles are summarized in Table 3. The monopile dimensions have been extracted from Medina et al. (2021), where its sizing has been addressed based on the procedure described by Arany et al. (2016).

Finally, the necessary inertial characteristics to reproduce the equivalent weight of the superstructure of these OWTs are indicated in Table 4. In this table, the masses of the different components of the system (Fig. 1(c)), the total mass of the superstructure (m), and the ultimate axial bearing capacity of the OWT monopiles (Q_u) are listed. Besides, to quantify this total mass with respect to the Q_u of each monopile and soil, the relation between these two parameters (δ) is also presented. Piles and the wind turbine are considered of S355 structural steel, whose main characteristics are: Young's modulus of 210 GPa, Poisson's ratio of 0.3 and density of 7850 kg/m^3. To determine the additional mass due to the interaction between pile and water, a density of sea water of 1030 kg/m^3 and a maximum water depth of 25 m have been considered.

3.4. Seismic signals

Ten accelerograms are used in this study, all of them obtained from the PEER Ground Motion Database (Pacific Earthquake Engineering Research Center (PEER), 2022). Table 5 provides the main information of each earthquake: the record sequence number (RSN) of the database, the direction with respect to the north of the horizontal component used, name and year of the earthquake event, name of the measuring station, the time-average shear-wave velocity for the upper 30 m depth ($V_{s,30}$) of the soils in which they have been measured, the maximum ground acceleration ($a_{g,max}$) and the time step (ΔT) of each signal.

Table 3
Main characteristics of the OWTs used in this work.
Source: Medina et al. (2021).

OWT	5 MW (Jonkman et al., 2009)	10 MW (Bak et al., 2013)	15 MW (Gaertner et al., 2020)
Tower height (m)	90	119	135
Rotor diameter (m)	126	178	240
Rated wind speed (m/s)	11.4	11.4	10.6
Cut-out wind speed (m/s)	25	25	25
Rotor operational speed range (rpm)	6.9–12.1	6–9.6	5–7.6
Tower top diameter (m)	3.9	5.5	6.5
Tower bottom diameter (m)	6	8.3	10
Tower top thickness (m)	0.019	0.020	0.024
Tower bottom thickness (m)	0.027	0.038	0.041
Pile diameter (m)	6.04	8.30	10.00
Pile thickness (m)	0.067	0.090	0.107
Pile length over mudline (m)	32.6	32.6	32.6
Pile embedded length (m)	49.7	63.8	73.8

Table 4
Inertial characteristics of the OWTs and its corresponding monopiles in the two soils studied in this work.

Mass (t)	5 MW	10 MW	15 MW
Rotor-nacelle assembly	350	674	1017
Tower	347.46	605	860
Substructure	321.74	594.05	851.04
Water inside substructure	703.38	1329.6	1931.1
Total weight [m]	1722.6	3202.7	4659.1
Loose			
Q_u (t) - Unplugged	8292.7	15 057	21 275
δ $[m/Q_u]$	0.208	0.213	0.219
Dense			
Q_u (t) - Unplugged	14 346	26 037	36 784
δ $[m/Q_u]$	0.120	0.123	0.127

Based on a convergence analysis, these time steps are the ones used to compute the system kinematic variables with the Newmark Method.

These acceleration signals are assumed to correspond to the free-field acceleration at surface level for all soil profiles. In order to make the structural response of all these seismic signals comparable to each other, the accelerograms are scaled to a maximum ground acceleration of 0.6 g. The system seismic response is computed as the average response of the ten accelerograms, following the DNV-RP-0585 guidelines (DNV, 2021), which recommends to evaluate the seismic design of wind power plants by computing the mean response of, at least, seven earthquakes.

4. Results and discussion

This section presents the comparative analysis carried out for the soil–pile subsystem (Fig. 1(b)) and its applicability to understand the behaviour of the complete OWT-monopile system (Fig. 1(c)).

Regarding the parametric analysis conducted using the soil–pile subsystem, the results are organized as follows:

- First, the mean envelopes of maximum seismic responses for three different piles without pile cap (soil–pile subsystem with $\delta = 0$) are studied (Fig. 3) with the aim of quantifying the non-linear and inelastic behaviour in the kinematic soil–pile interaction problem.
- Secondly, these same envelopes are analysed for the same piles with a cap mass equivalent to its ultimate axial bearing capacities ($\delta = 1$, Fig. 4) in order to study the inertial interaction effect within soil–pile non-linear and plastic behaviour.
- Next, the soil resistance temporal evolution in each model at two different depths is presented in Figs. 5 and 6 for the two previous configurations in order to illustrate the activation of the non-linear an plastic behaviours.
- After that, the contribution of the inertial effect within soil–pile interaction is analysed for several piles and δ values, computing the relative differences of the maximum seismic responses of each model with respect to those of the linear one (Figs. 7–9).

Finally, the mean envelopes of maximum seismic responses of three different monopiled OWTs are studied and compared with the envelopes of its corresponding monopiles with a pile cap mass equivalent to the weight of each supported OWT (Fig. 10) in order to verify the conclusions of the parametric analysis.

4.1. Envelopes of maximum seismic responses

Fig. 3 shows the mean envelopes of maximum bending moments (M), shear forces (V), accelerations (a) and soil resistances (P) for the three diameters (D) considered. These results correspond to the soil–pile subsystem (Fig. 1(b)) without pile cap mass ($\delta = 0$) and with a pile length of 30 m. Results of each response variable are disposed by columns, while those corresponding to the diameters are arranged by rows. Each subgraph is divided into two parts separated by a line of points and dashes: the envelopes corresponding to the medium dense sandy soil (Dense) and the very loose one (Loose) are shown on left and right sides, respectively. The depth and the envelopes values are represented on y-axis and x-axis accordingly. The envelopes obtained in the different considered models (NDLM, ENLM, PNLM) are distinguished with different colours. In the envelopes corresponding to the soil resistance (fourth column), an additional green curve is included to represent the ultimate lateral resistance of the soil (P_u).

In Fig. 3 it can be observed that virtually the same results between the three models are obtained for all diameters and response variables studied. Thus, in this case without pile cap mass, where the kinematic effects governs the soil–pile interaction, the consideration of a non-linear and inelastic soil–pile interaction model seems to be irrelevant, so a linear elastic model is enough to reproduce the soil–pile kinematic response.

Regarding the influence of the soil type, it can be appreciated that greater bending moments and shear forces are reached in the Loose soil, while higher accelerations are obtained in the Dense one. As the diameter increases, greater internal forces and lower acceleration envelopes are found. The maximum bending moments and accelerations are obtained at pile head, however, the maximum shear forces are reached at shallow levels, increasing this depth when the pile diameter grows. With respect to the soil resistance envelopes (fourth column of Fig. 3), it can be seen that the ultimate lateral bearing capacity of soil (p_u) is not reached in any case. In fact, the soil resistance is quite smaller than the value of the ultimate resistance at the different depths, approaching the limit only near the free surface level. This fact, will be further studied in Section 4.2.

To analyse the effect of the inertial interaction within soil–pile dynamic interaction, the same envelopes than those presented in Fig. 3

Table 5
Information about the seismic signals (accelerograms) used in this work.
Source: Pacific Earthquake Engineering Research Center (PEER) (2022).

RSN	Dir. (°)	Event name	Year	Station name	$V_{S,30}$ (m/s)	$a_{g,max}$ (g)	Δt (s)
186	90	Imperial Valley-06	1979	Niland Fire Station	212	0.11	0.005
266	102	Victoria Mexico	1980	Chihuahua	242	0.15	0.010
729	0	Superstition Hills-02	1987	Imperial Valley W.L.A	179	0.21	0.005
1176	60	Kocaeli Turkey	1999	Yarimca	297	0.23	0.005
1498	59	Chi-Chi Taiwan	1999	TCU059	273	0.16	0.005
1792	90	Hector Mine	1999	Indio-Riverside C.F.G	282	0.12	0.010
2715	47	Chi-Chi Taiwan-04	1999	CHY047	170	0.13	0.004
3683	11	Taiwan SMART1(45)	1986	SMART1 O11	295	0.13	0.010
3965	8	Tottori Japan	2000	TTR008	139	0.32	0.010
5666	7	Iwate Japan	2008	MYG007	167	0.13	0.010

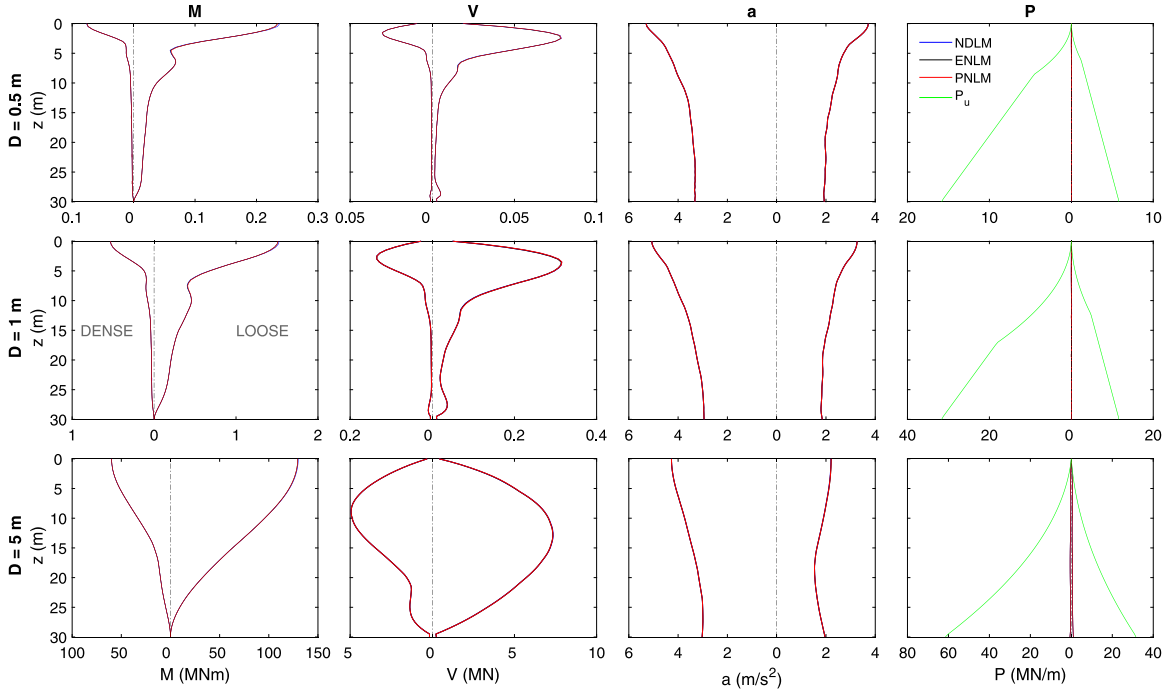

Fig. 3. Mean envelopes of maximum seismic responses for the soil–pile subsystem without a cap mass ($\delta = 0$).

but with a pile cap mass equivalent to the ultimate axial bearing capacity of each pile ($\delta = 1$) are shown in Fig. 4. The same graph distribution that the one previously used for Fig. 3 is also employed in Fig. 4.

In Fig. 4 remarkable differences between the envelopes obtained in the three different models are seen. So, the non-linear and inelastic behaviour of soil–pile dynamic interaction becomes relevant when the inertial interaction is activated by the dynamic excitation. For lower diameters (0.5 and 1 m), greater differences between the envelopes of the three models can be distinguished; while for the diameter of 5 m, the envelopes are very similar between the three models. The highest maximum value of the seismic responses (that are obtained at pile head for bending moments, shear forces and accelerations) are found for the linear model (NDLM) in the pile diameters of 0.5 and 1 m. Thus, in terms of maximum seismic responses, the NDLM is a conservative assumption for lower diameters.

Comparing the responses corresponding to the plastic and elastic non-linear models (PNLM and ENLM), very similar envelopes are obtained. Only in the acceleration envelopes of the diameters 0.5 and 1 m, and for the Dense soil, a relevant difference between these two models can be observed. Higher envelopes are reached in the ENLM for the two soils and the three diameters. Thus, although the consideration of an elastic and plastic non-linear model leads to similar structural-seismic responses, the elastic non-linear approach seems to be the most conservative between these two.

Regarding the highest responses values, these are generally computed at pile head for the internal forces and accelerations. Furthermore, greater internal forces, accelerations and soil resistances are obtained when a Dense soil is defined, a contrary trend to what has been obtained when the pile cap mass is not considered (Fig. 3), where greater internal forces are computed in the Loose soil.

According to the soil resistance envelopes, for the shallower depths, the soil resistance corresponding to the Non-Degraded Linear Model overpasses the ultimate lateral bearing capacity of soil (p_u), while in the non-linear plastic and elastic models the soil ultimate lateral bearing capacity is reached in these same depths (note that the soil resistance in these two models are limited to the p_u value). Furthermore, it can be observed that the soil resistance of the linear model exceeds p_u to a greater extent as the diameter becomes smaller. This fact justifies the remarkable differences between the linear and the two non-linear models for the diameters of 0.5 and 1 m. Finally, it is important to highlight that the differences between the three models are obtained in the shallower depths, that is, in the same soil levels where the ultimate lateral bearing capacity is exceeded by the linear model.

4.2. Evolution of soil resistance

To better understand the differences between the two non-linear models and the linear one in the soil–pile subsystem without and with

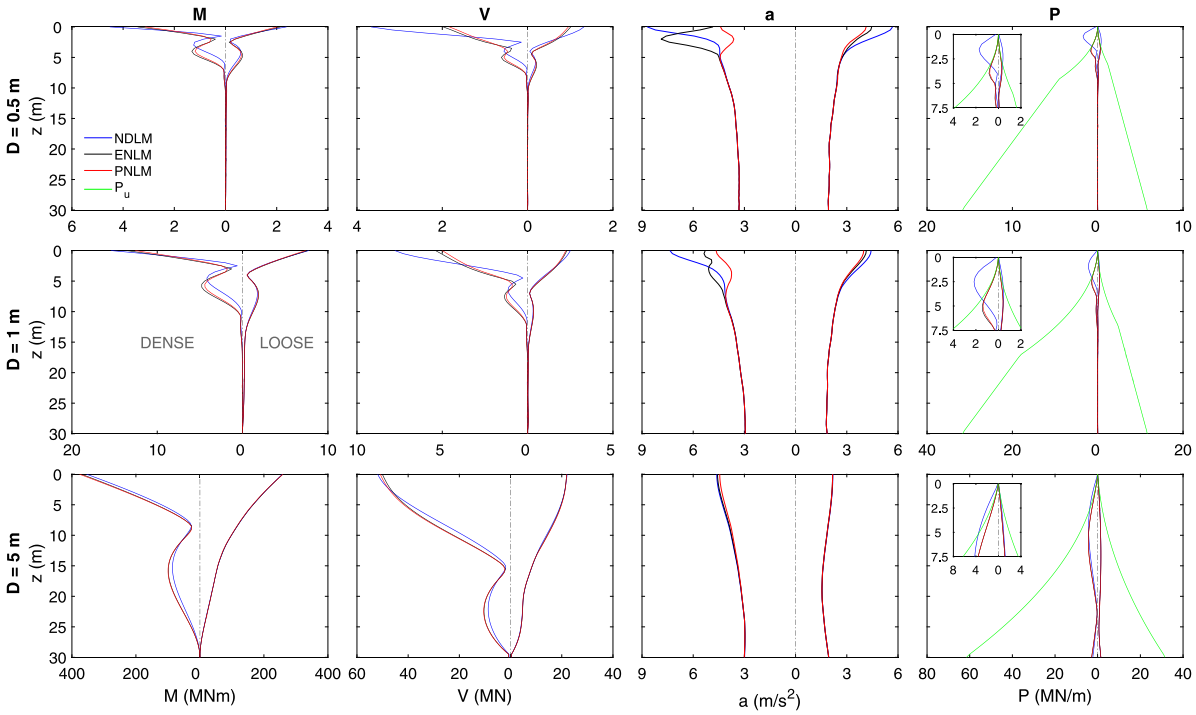

Fig. 4. Mean envelopes of maximum seismic responses considering a mass equal to the ultimate axial bearing capacity ($\delta = 1$).

pile cap mass previously studied in Section 4.1, the evolution of soil resistance (P, y-axis) with respect to the soil–pile deflection ($\tilde{y}$, x-axis) at pile head and at depth equal to a diameter are represented in Figs. 5 and 6. These results correspond to the same earthquake event: the Imperial Valley signal (see Table 5). Fig. 5 shows the temporal evolutions for the subsystem without pile cap mass ($\delta = 0$), while Fig. 6 those corresponding to the subsystem with pile cap mass equal to the ultimate axial pile bearing capacity ($\delta = 1$). In both figures, results of the three diameters are presented by columns, and those corresponding to the two depths and soils are shown by rows: the two upper rows presents the results of the Loose soil and the two bottom ones, those of the Dense soil. The soil resistance evolution at pile head and at a depth equal to the pile diameter are disposed in the first and second row of each soil, accordingly. By using different colours the three models are distinguished.

The temporal evolutions of the p-y relation clearly show the non-linear behaviour of the plastic (red curve) and elastic non-linear models (black curve). When only the kinematic interaction effect is analysed (Fig. 5), the three models reach similar values of maximum soil resistances and soil–pile deflections, except for the soil resistances at pile head for the diameters of 0.5 and 1 m, where the maximum values correspond to the Non-Degraded Linear Model. When the diameter and depth increases, the evolution of soil resistance of non-linear models tend to assimilate to the evolution obtained in the linear model, indicating that the ultimate lateral bearing capacity is far from being reached. Higher soil resistances and soil–pile deflections are found for the Loose soil, in agreement with the previous results in terms of envelopes (Fig. 3). When a Dense soil is considered, for a depth equivalent to the pile diameter, the evolution of soil resistance for the non-linear models is practically linear.

When a pile cap mass equivalent to the ultimate axial bearing capacity of pile is considered ($\delta = 1$, Fig. 6), high differences are obtained between the soil resistances of the two non-linear models with respect to the linear one. For the small diameters (0.5 and 1 m), the soil resistances of the linear model greatly exceed the ultimate lateral soil resistance. Furthermore, contrary to what has been stated for Fig. 5, the maximum soil resistance values are obtained for the Dense soil, where a remarkable difference between the maximum values of the linear and non-linear models can be appreciated. Note that these trends coincide with the ones for the envelopes with $\delta = 1$ (Fig. 4).

4.3. Relative differences with respect to the non-degraded linear model

With the aim of comparing the three models for different δ values, the relative differences between the maximum results of the non-linear models (ENLM and PNLM) with respect to those obtained in the non-degraded linear model (NDLM) are depicted in Figs. 7–9. The differences of maximum mean bending moments (M), shear forces (V), accelerations (a) and soil resistances (P) are arranged by columns; while the different two soil profiles are placed in rows. In all these representations, the relative differences (y-axis) with respect to the different value of δ (x-axis) are shown. The results corresponding to the PNLM and ENLM are presented in different colours.

In Fig. 7, the relative differences of the maximum responses for the subsystem with a pile diameter of 1 m and a length of 30 m are shown. The relative differences corresponding to the ten seismic signals are depicted with points, while the relative differences of the maximum mean responses of the ten seismic signals are presented with a continuous line. Analysing the relative differences of the maximum mean responses, it can be appreciated that in the Loose soil similar results between the non-linear models and the linear one are obtained for δ values lower or equal than 0.5. When δ increases, relevant relative differences are obtained, reaching values between 5 and 10% for the internal forces, accelerations and soil resistances in the highest values of δ. Regarding the Dense soil, important relative differences can be observed from δ values higher than 0.25. The differences computed in the Dense soil are approximately three and four times greater than those of the Loose one, reaching values over a 30%. In both soils, once the inertial interaction effect acquires relevance, the relative differences of the Plastic Non-Linear Model (PNLM) are higher than those of the Elastic Non-Linear Model (ENLM). However, these relative differences are, in general, negative, indicating that the Non-Degraded Linear Model (NDLM) is the most conservative in terms of maximum seismic responses.

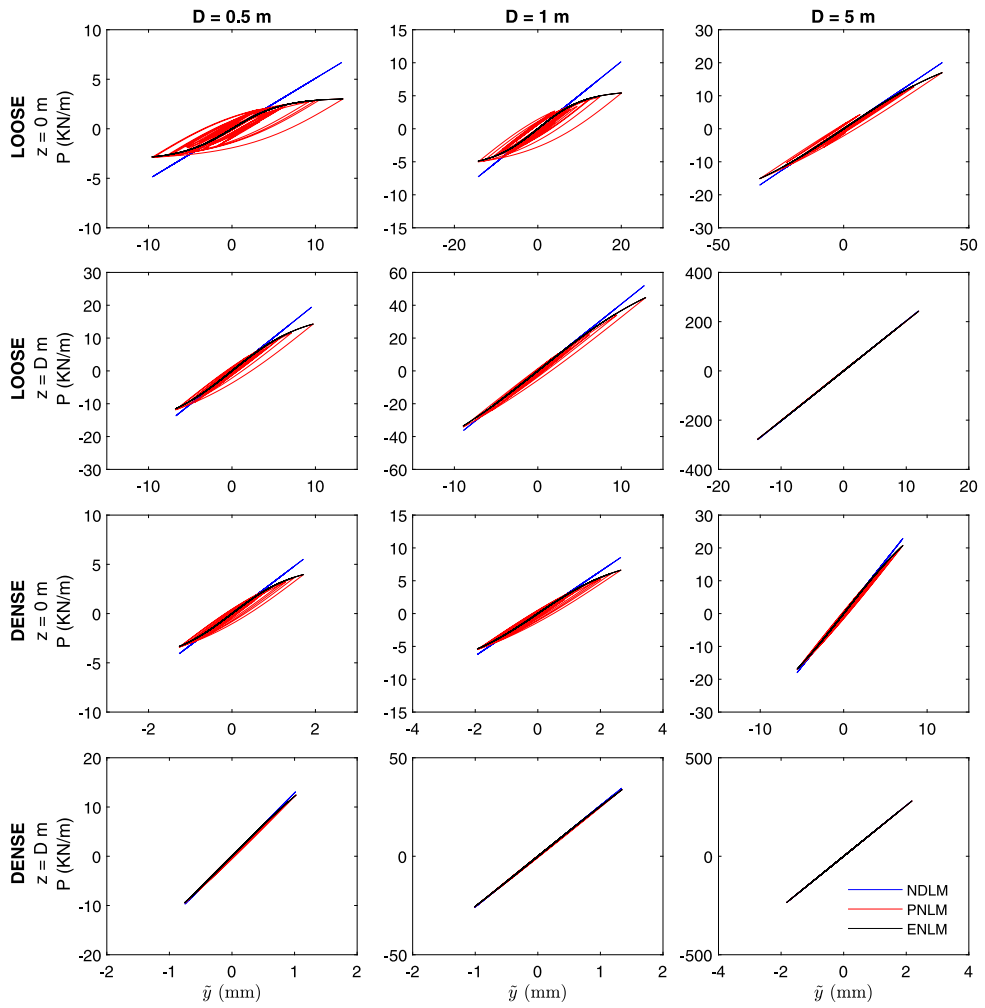

Fig. 5. Evolution of soil resistance (P) versus soil–pile relative displacement ($\tilde{y}$), for $\delta = 0$. Results for the Imperial Valley signal.

Attending to the relative differences of each earthquake, it can be observed that some differences are positive for a few seismic signals in the bending moments and soil resistances. Furthermore, it can be seen that several seismic excitations leads to remarkable higher and lower differences than the ones obtained for the maximum mean responses, justifying the importance of considering the mean response of at least seven earthquakes (as it is recommended in the DNV-RP-0585 guideline DNV, 2021). Also, it can be observed that for large values of δ the dispersion of the results tends to increase.

Fig. 8 shows the relative differences for the three pile diameters studied, all of them with a pile length of 30 m. By using different types of lines the results of each diameter are distinguished. The highest relative differences are reached for the lowest pile diameters, following a similar trend to what Tabesh and Poulos (2001) exposes. Besides, for small pile diameters, lower δ values are required to obtain relevant differences between the linear and non-linear models. Note how for a pile diameter of 0.5 m and δ values greater than 0.25, significant relative differences appear. The relative differences in the three diameters are mostly negative, excepting the bending moments and soil resistances of the 5 m pile diameter. For this pile diameter, negligible relative differences (lower than 5%) are generally obtained in the entire δ interval, excepting the bending moment and soil resistance differences for the highest δ values. For all diameters and δ values, greater relative differences are reached in the Plastic Non-Linear Model. As it has been previously commented, in the Dense soil higher differences are generally reached compared to the Loose one.

The relative differences corresponding to the soil–pile subsystem with a diameter of 1 m and three different pile lengths (15, 30 and 60 m) are represented in Fig. 9. Different line plots are used to distinguish the three lengths studied. The highest differences are reached for large pile lengths. A similar trend in the results than the ones previously commented is generally obtained: the differences are mostly negative and the Plastic Non-Linear Model leads to the highest relative differences; the bending moment and soil resistance relative differences are sometimes positive for a length of 15 m, a similar trend to those it has been obtained for the differences of the 5 m pile diameter (previously shown in Fig. 8). In conclusion, for non-slender piles, the non-linear models lead to a greater response than the linear one in terms of bending moments and soil resistances if the inertial effects are activated.

4.4. Envelopes of monopiled OWTs and its corresponding monopiles

Fig. 10 shows the mean envelopes of maximum bending moments (M), shear forces (V) and accelerations (a), for three monopiled OWTs with rated powers of 5, 10 and 15 MW obtained by the integrated model including OWT superstructure, (Fig. 1(c)) and its corresponding monopiles subsystems, with a pile cap mass equivalent to its supported superstructure weight (see Table 4). The different response variables are arranged by columns, while the envelopes corresponding to each OWT are disposed by rows. The same results disposal than the ones previously used for the envelopes of Figs. 3 and 4 is employed: the envelopes corresponding to the dense and the loose soil are shown on left and right side respectively (separated by a vertical line); the envelopes obtained in the different models considered (NDLM, ENLM,

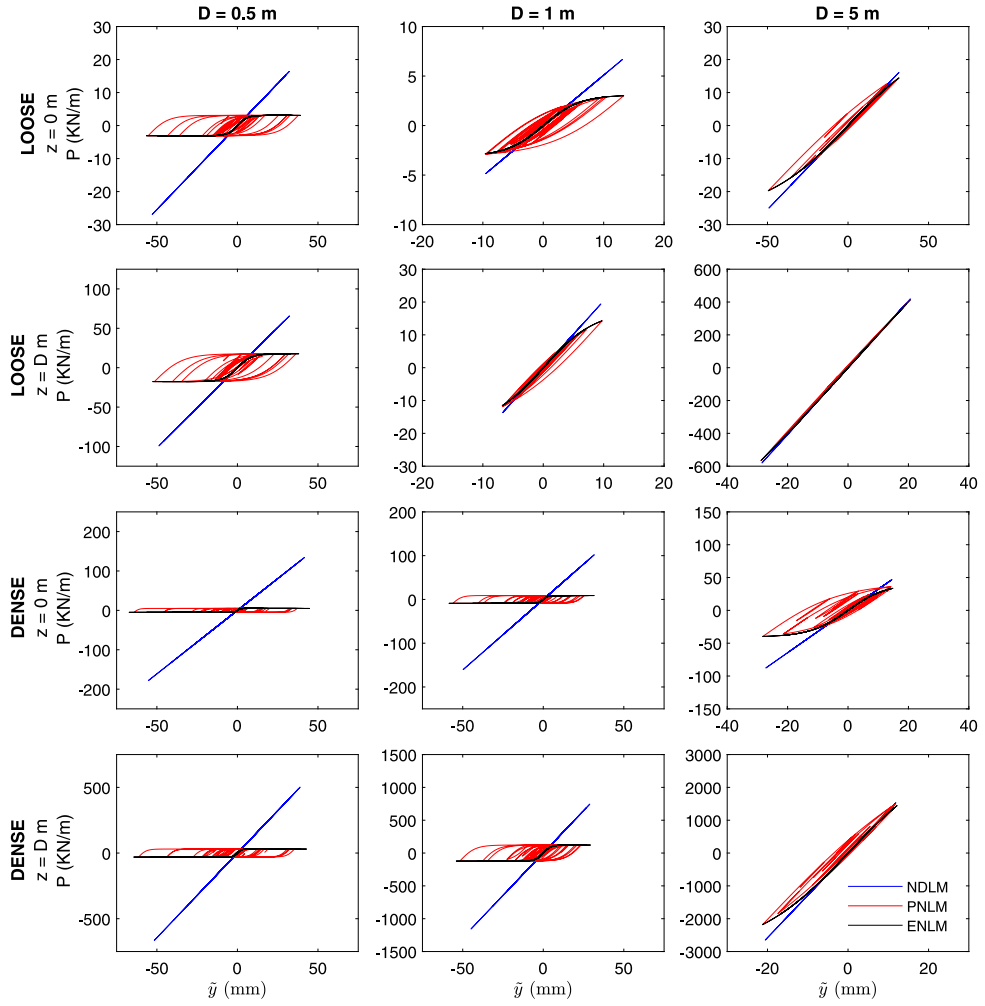

Fig. 6. Evolution of soil resistance (P) versus soil–pile relative displacement ($\tilde{y}$), for $\delta = 1$. results for the Imperial Valley signal.

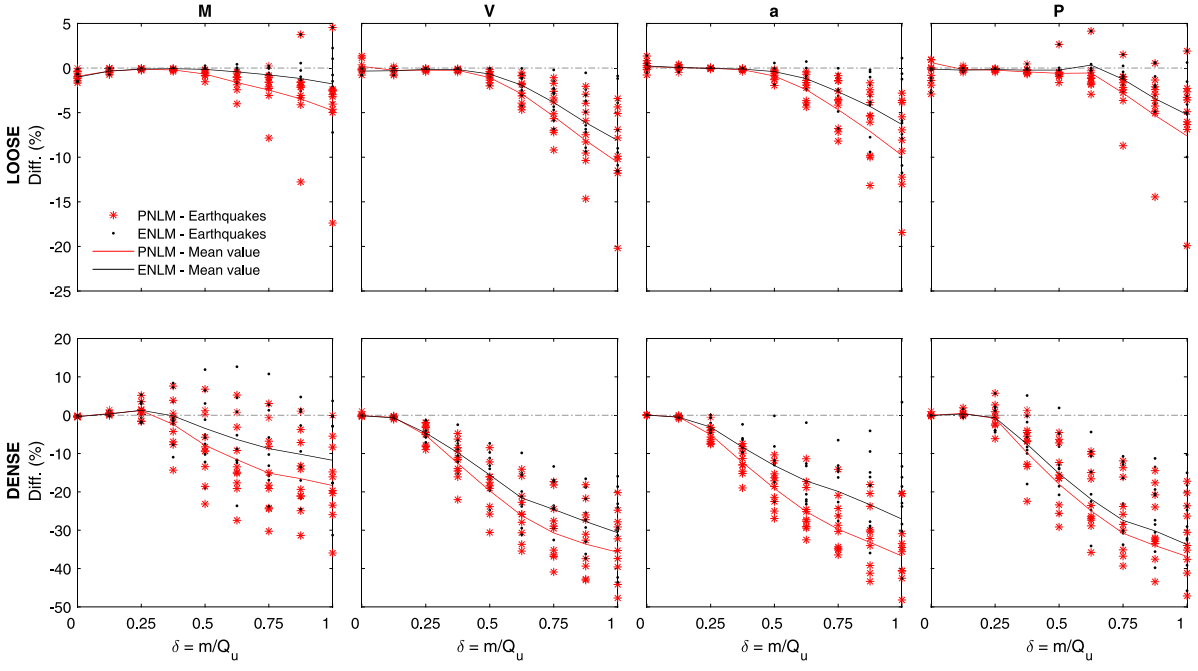

Fig. 7. Relative differences of maximum results of each earthquake with respect to those of the NDLM.

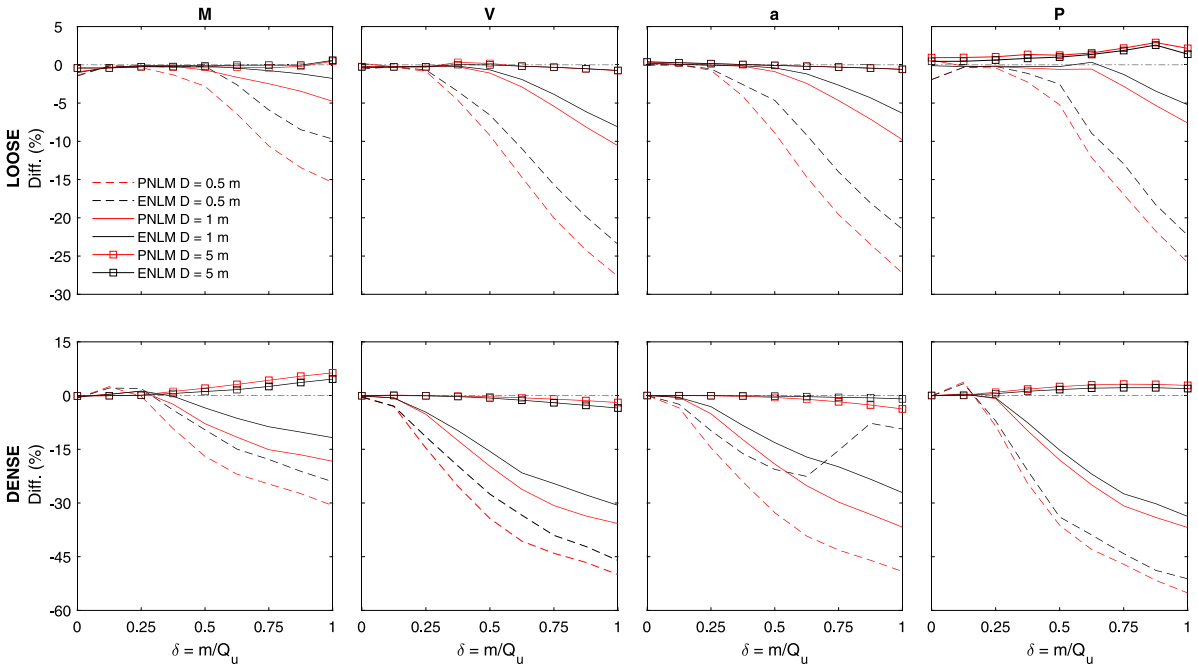

Fig. 8. Relative differences of mean maximum results with respect to those of the NDLM, for several pile diameters ($L = 30$ m).

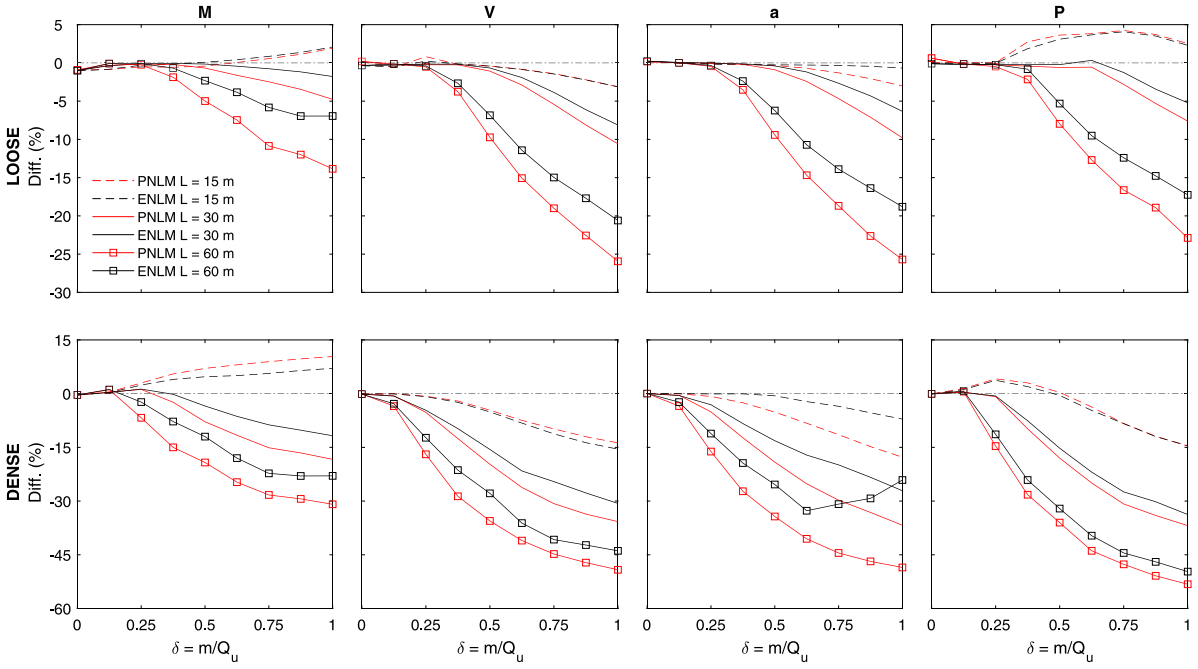

Fig. 9. Relative differences of mean maximum results with respect to those of the NDLM, for several pile lengths ($D = 1$ m).

PNLM) are distinguished with different colours. Two dashed horizontal lines are used to represent the seabed surface (yellow line) and the height of the substructure (blue line). The envelopes for the soil–pile subsystems are presented by dotted lines.

In Fig. 10 it can be observed that similar envelopes are obtained for the three models studied. Note that the equivalent δ value of these superstructures and its corresponding monopiles are around 0.2 and 0.12 for the Loose and Dense soil respectively (see Table 4). As presented in Section 4.3, these values correspond to the δ range for which the non-linearity of the soil–pile interaction has no relevance. Some small differences can be observed between the linear and non-linear models in the envelopes of the Dense soil, where the results of the Non-Degraded Linear Model are slightly larger than those of the non-linear models. In terms of the global foundation-structure-OWT system seismic response, the linear elastic model for soil–pile interaction is conservative, as it has been obtained throughout this study.

Comparing the envelopes of the entire system (OWT and monopiles) with those of the monopiles and the equivalent pile cap OWT masses, greater maximum internal forces are obtained for the Dense soil when the entire system is considered, while in the Loose soil higher internal forces values are reached in the single monopile configuration. With respect to the kinematic variables studied (displacements and accelerations), similar envelopes are computed in the two configurations. Note

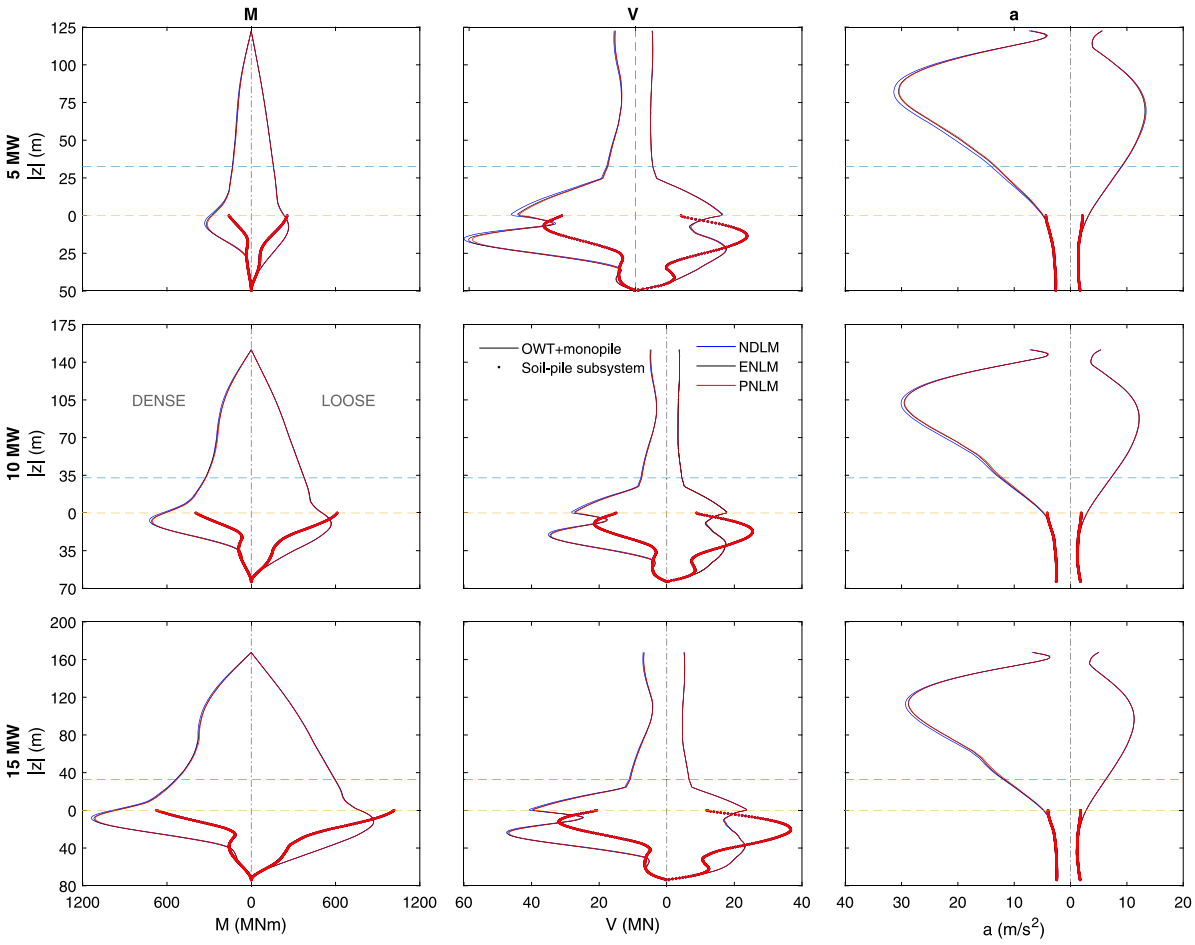

Fig. 10. Mean envelopes of maximum seismic responses for the monopiled OWTs and its corresponding soil–pile subsystems.

that the principal difference between the two models is the pile head rotation restriction that is imposed in the soil–pile subsystem.

5. Conclusions

This paper studies the influence of non-linearity and plasticity of soil–pile interaction on the seismic response of OWT pile foundations embedded in two different types of sandy soils. For this purpose, three different models: a Plastic Non-Linear, an Elastic Non-Linear and a Non-Degraded Linear Model are analysed and compared. These three models reproduce the soil–pile interaction by a Beam on Dynamic Winkler Foundation approach based on the *p-y* curves established by the API RP 2A-WSD. An incident field for non-homogeneous medium with linear variation of soil properties is contemplated in each soil–pile model. Characteristic pile geometries of jacket and monopile foundations embedded in very loose and medium dense sandy soils are studied. The effects of the non-linear and plastic assumptions are analysed by evaluating the kinematic and inertial effects within soil–pile interaction. For this purpose, different translational cap masses are studied in a soil–pile subsystem. From the analysis of the envelopes of maximum responses and its relative differences with respect to the linear model, the following conclusions are drawn:

- Similar results between models are obtained when the kinematic interaction effect predominates within soil–pile dynamic interaction. Thus, the consideration of a linear elastic model is enough to reproduce the soil–pile kinematic interaction.
- The non-linear and inelastic behaviour of soil–pile dynamic interaction acquires relevance when the inertial interaction is excited. Nevertheless, the consideration of a linear elastic model leads generally to higher maximum seismic responses.
- Similar seismic responses are obtained by considering a plastic or elastic non-linear model. Between these two models, greater responses are found in the elastic non-linear one. For this reason, if a non-linear model must be used, it is enough to consider an elastic soil–pile interaction, avoiding the complexity of the cyclic behaviour of soil–pile interaction.
- Greater internal forces are obtained in soft (Loose) soils when the kinematic interaction effect prevails, while when the inertial interaction predominates higher internal forces are computed in stiffer (Dense) soils.
- Higher differences between models are produced for small-diameter slender piles and in the Dense soil. These differences arise because the ultimate lateral resistance is greatly exceeded in the Non-Degraded Linear Model.

The main conclusions drawn of the analysis of the soil–pile subsystems are tested with three reference OWTs, comparing its envelopes of maximum responses with those of its corresponding monopiles with a pile cap mass equivalent to the superstructure mass.

- For these configurations, similar envelopes of maximum bending moments, shear forces and accelerations between models are obtained, as the mass of the superstructure is not enough to activate the inertial interaction effects.

Therefore, focusing on the soil–pile interaction phenomena, when the kinematic interaction dominates and a linear incident field is

considered, an elastic linear Winkler model formulated through non-degraded soil properties allows to reach accurate and conservative seismic responses. This is a general and interesting conclusion due to the simplicity of the proposed solution and it has been fully demonstrated with an extensive study of problems and excitations. By means of a simple model that reduces the complexity of the soil–pile interaction phenomena, it is possible to obtain accurate and conservative results. As a second phase of the two non-linear models and the work carried out, it is necessary to incorporate the non-linear behaviour of the incident field and to compare it with the linear assumption. On this manner, it can be evaluated to what extent a linear model is accurate enough to reproduce the system seismic response, or how it should be modified to adjust to that response. In this respect, there are very interesting recent works, see e.g Stacul et al. (2022), which, from a different approach and less specific analysis, obtain conclusions that follow a similar trend to what has been obtained in this study: the kinematic pile seismic response is mainly influenced by the model stiffness, rather than by the non-linear or inelastic behaviour of free field response and soil–pile interaction.

CRediT authorship contribution statement

Eduardo Rodríguez-Galván: Writing – original draft, Visualization, Software, Methodology, Conceptualization. **Guillermo M. Álamo:** Writing – review & editing, Software, Conceptualization. **Juan J. Aznárez:** Writing – review & editing, Supervision, Funding acquisition, Conceptualization. **Orlando Maeso:** Writing – review & editing, Supervision, Conceptualization.

Declaration of competing interest

The authors declare that they have no known competing financial interests or personal relationships that could have appeared to influence the work reported in this paper.

Data availability

Data will be made available on request.

Acknowledgements

This research has been funded by Ministerio de Ciencia e Innovación and Agencia Estatal de Investigación (MCIN/AEI/10.13039/501100011033) of Spain and FEDER through research project PID2020-120102RBI00 and predoctoral research scholarship PRE2021-099200 (E. Rodríguez-Galván), also funded by FSE+. This research has been partially supported by ACIISI, Spain-Gobierno de Canarias and European FEDER Funds Grant EIS 2021 04.

References

Álamo, G.M., Aznárez, J.J., Padrón, L.A., Martínez-Castro, A.E., Gallego, R., Maeso, O., 2018. Dynamic soil-structure interaction in offshore wind turbines on monopiles in layered seabed based on real data. Ocean Eng. 156, 14–24.

Álamo, G.M., Bordón, J.D.R., Aznárez, J.J., 2021. On the application of the beam model for linear dynamic analysis of pile and suction caisson foundations for offshore wind turbines. Comput. Geotech. 134, 104107.

Alati, N., Failla, G., Arena, F., 2015. Seismic analysis of offshore wind turbines on bottom-fixed support structures. Phil. Trans. R. Soc. A 373 (2035), 20140086.

Arany, L., Bhattacharya, S., Macdonald, J.H.G., Hogan, S.J., 2016. Closed form solution of eigen frequency of monopile supported offshore wind turbines in deeper waters incorporating stiffness of substructure and SSI. Soil Dyn. Earthq. Eng. 83, 18–32.

Bak, C., Zahle, F., Bitsche, R., Kim, T., Yde, A., Henriksen, L.C., Natarajan, A., Hansen, M., 2013. Description of the DTU 10 MW reference wind turbine. In: DTU Wind Energy Report-I-0092. Vol. 5, DTU Wind Energy.

Bisoi, S., Haldar, S., 2014. Dynamic analysis of offshore wind turbine in clay considering soil–monopile–tower interaction. Soil Dyn. Earthq. Eng. 63, 19–35.

Bisoi, S., Haldar, S., 2015. Design of monopile supported offshore wind turbine in clay considering dynamic soil–structure-interaction. Soil Dyn. Earthq. Eng. 73, 103–117.

BOSLAN Engineering and Consulting, 2022. The Next Generation Monopile Foundations for Offshore Wind Turbines - Manufacturing , Design and Handling Challenges. Technical report.

Carswell, W., Arwade, S.R., DeGroot, D.J., Myers, A.T., 2016. Natural frequency degradation and permanent accumulated rotation for offshore wind turbine monopiles in clay. Renew. Energy 97, 319–330.

Chen, L., Wu, W., Liu, H., Hu, A., Newson, T., El Naggar, M.H., Mei, G., Xu, M., 2022. Analytical solution for lateral vibration of offshore pipe piles considering hydrodynamic pressure. Comput. Geotech. 151, 104962.

Cheng, X., Wang, T., Zhang, J., Wang, P., Tu, W., Li, W., 2023. Dynamic response analysis of monopile offshore wind turbines to seismic and environmental loading considering the stiffness degradation of clay. Comput. Geotech. 155, 105210.

Chopra, A.K., 2011. Dynamics of Structures: Theory and Applications To Earthquake Engineering, Fourth Prentice-Hall International Series in Civil Engineering and Engineering Mechanics.

Designing API RP 2A-WSD, Recommended Practice for Planning and Constructing Fixed Offshore Plaftorms - Working Stress Design. American Petroleum Institute.

DNV, 2014a. Design of offshore wind turbine structures. Offshore Standard DNV-OS-J101. Det-Norske Veritas AS.

DNV, 2014b. Environmental conditions and environmental loads. Recommended Practice DNV-RP-C205. Det-Norske Veritas AS.

DNV, 2021. Seismic design of wind power plants. Recommended Practice DNV-RP-0585. Det-Norske Veritas AS.

Firoj, M., Maheshwari, B.K., 2022. A new nonlinear spring-dashpot model of CPRF of NPP structure based on coupled BEM-FEM approach. Earthq. Eng. Struct. Dyn..

Gaertner, E., Rinker, J., Sethuraman, L., Zahle, F., Anderson, B., Barter, G., Abbas, N., Meng, F., Bortolotti, P., Skrzypinski, W., et al., 2020. Definition of the IEA 15-megawatt offshore reference wind turbine.

Gazetas, G., Dobry, R., 1984. Simple radiation damping model for piles and footings. J. Eng. Mech. 110 (6), 937–956.

Gerolymos, N., Gazetas, G., 2005a. Constitutive model for 1-D cyclic soil behaviour applied to seismic analysis of layered deposits. Soils Found. 45 (3), 147–159.

Gerolymos, N., Gazetas, G., 2005b. Phenomenological model applied to inelastic response of soil-pile interaction systems. Soils Found. 45 (4), 119–132.

Hassan, A.M., 2018. Winkler model for pile seismic analysis considering end constraints effects. HBRC J. 14 (3), 316–320.

Jiang, W., Lin, C., 2022. Lateral responses of monopile-supported offshore wind turbines in sands under combined effects of scour and earthquakes. Soil Dyn. Earthq. Eng. 155, 107193.

Jiang, W., Lin, C., Sun, M., 2021. Seismic responses of monopile-supported offshore wind turbines in soft clays under scoured conditions. Soil Dyn. Earthq. Eng. 142, 106549.

Jonkman, J., Butterfield, S., Musial, W., Scott, G., 2009. Definition of a 5-MW Reference Wind Turbine for Offshore System Development. Technical report, National Renewable Energy Lab.(NREL), Golden, CO (United States).

Jonkman, J., Musial, W., 2010. Offshore Code Comparison Collaboration (OC3) for IEA Wind Task 23 Offshore Wind Technology and Deployment. Technical report, National Renewable Energy Lab.(NREL), Golden, CO (United States).

Ju, S.H., Huang, Y.C., 2019. Analyses of offshore wind turbine structures with soil-structure interaction under earthquakes. Ocean Eng. 187, 106190.

Kaynia, A.M., 2021. Effect of kinematic interaction on seismic response of offshore wind turbines on monopiles. Earthq. Eng. Struct. Dyn. 50 (3), 777–790.

Kramer, S.L., 1996. Geotechnical Earthquake Engineering. Prentice-Hall International Series in Civil Engineering and Engineering Mechanics, ISBN: 0-13-374943-6,

Liang, F., Yuan, Z., Liang, X., Zhang, H., 2022. Seismic response of monopile-supported offshore wind turbines under combined wind, wave and hydrodynamic loads at scoured sites. Comput. Geotech. 144, 104640.

Medina, C., Álamo, G.M., Quevedo-Reina, R., 2021. Evolution of the seismic response of monopile-supported offshore wind turbines of increasing size from 5 to 15 MW including dynamic soil-structure interaction. J. Mar. Sci. Eng. 9 (11), 1285.

Mo, R., Cao, R., Liu, M., Li, M., 2021. Effect of ground motion directionality on seismic dynamic responses of monopile offshore wind turbines. Renew. Energy 175, 179–199.

Musial, W., Spitsen, P., Duffy, P., Beiter, P., Marquis, M., Hammond, R., Shields, M., 2022. Offshore Wind Market Report: 2022 Edition. Technical report, National Renewable Energy Lab.(NREL), Golden, CO (United States).

Pacific Earthquake Engineering Research Center (PEER), 2022. NGA-West2 Ground Motion Database. Accessed on 20 August 2022. Available online: ngawest2.berkeley.edu/.

Padrón, L.A., Carbonari, S., Dezi, F., Morici, M., Bordón, J.D.R., Leoni, G., 2022. Seismic response of large offshore wind turbines on monopile foundations including dynamic soil–structure interaction. Ocean Eng. 257, 111653.

Patra, S., Haldar, S., 2021. Seismic response of monopile supported offshore wind turbine in liquefiable soil. In: Structures. Vol. 31, Elsevier, pp. 248–265.

Rovithis, E.N., Parashakis, H., Mylonakis, G.E., 2011. 1D harmonic response of layered inhomogeneous soil: Analytical investigation. Soil Dyn. Earthq. Eng. 31 (7), 879–890.

Shi, S., Zhai, E., Xu, C., Iqbal, K., Sun, Y., Wang, S., 2022. Influence of pile-soil interaction on dynamic properties and response of offshore wind turbine with monopile foundation in sand site. Appl. Ocean Res. 126, 103279.

Stacul, S., Rovithis, E., Di Laora, R., 2022. Kinematic soil–pile interaction under earthquake-induced nonlinear soil and pile behavior: An equivalent-linear approach. J. Geotech. Geoenviron. Eng. 148 (7), 04022055.

Tabesh, A., Poulos, H.G., 2001. The effects of soil yielding on seismic response of single piles. Soils Found. 41 (3), 1–16.

Wang, Y., Zhang, Z., Wu, X., Zhu, B., Chen, Y., 2023. The py model of single pile foundation for OWTs under combined lateral environment loading and earthquake in saturated sand. Ocean Eng. 268, 113406.

Wang, P., Zhao, M., Du, X., Liu, J., Xu, C., 2018. Wind, wave and earthquake responses of offshore wind turbine on monopile foundation in clay. Soil Dyn. Earthq. Eng. 113, 47–57.

Xi, R., Xu, C., Du, X., El Naggar, M.H., Wang, P., Liu, L., Zhai, E., 2022. Framework for dynamic response analysis of monopile supported offshore wind turbine excited by combined wind-wave-earthquake loading. Ocean Eng. 247, 110743.

Yan, Y., Yang, Y., Bashir, M., Li, C., Wang, J., 2022. Dynamic analysis of 10 MW offshore wind turbines with different support structures subjected to earthquake loadings. Renew. Energy 193, 758–777.

Yang, Y., Bashir, M., Li, C., Wang, J., 2019. Analysis of seismic behaviour of an offshore wind turbine with a flexible foundation. Ocean Eng. 178, 215–228.